(Received 13 March 2025, Accepted 21 April 2025, Scheduled 29 April 2025)

Compound Dielectric Resonator Antenna

Alexander P. Volkov[1,*], Andrey Kobyakov[2], and David R. Peters[2]

[1] Corning Scientific Center, Helsinki, Finland
[2] Corning Research and Development Corporation, Corning Inc., Corning, NY, USA

ABSTRACT: A dielectric resonator antenna (DRA) with the resonator body formed, or compounded, by multiple building blocks is proposed. The approach gives flexibility in adjusting the resonator's shape to control input impedance and resonance frequency of the antenna. A simplified method of attaching the resonator's building blocks to the grounded dielectric substrate allowed for reduced fabrication complexity and manual reconfigurability of this compound DRA (cDRA). Several cDRAs with variable resonator sizes were studied theoretically and experimentally.

1. INTRODUCTION

Dielectric resonator antennas (DRAs) have been thoroughly investigated over the past three decades [1–4]. They remain in the focus of research due to a variety of promising applications, e.g., 5G/6G communication systems [5–9], energy harvesting [10], THz imaging [11], and implantable medical devices [12]. DRAs have a compact size, wide range of operation frequencies, relatively broad bandwidth, and high power-handling capacity. A DRA consists of a feeding structure (coaxial probe or slot in the ground plane) coupled to a dielectric resonator. The shape, size, and permittivity of the resonator critically affect radiation properties of the DRA, and thus numerous resonator shapes and compositions were studied in the past. Specifically, DRAs' design via resonator shape was addressed through the use of stacked resonators [13, 14] or more complex geometries: H-shape [15], stair-shape [16], resonators with an air tunnel [17]. Recently, new techniques for resonator shape optimization were proposed including both smooth [5, 18] and discrete, or fractal-like, resonators [19–21] which is sometimes represented as a collection of voxels [22].

Even though new materials and fabrication methods [5, 8, 23, 24] help improving DRAs' performance, antennas of this type have not yet reached a similarly broad application space as, for example, printed antennas. One of the reasons is fabrication complexity and the associated cost. Manufacturing a customized resonator shape for specific modal properties is challenging because high-permittivity materials are usually mechanically hard. Additional processing may also be required to drill a hole to effectively excite the resonator by a probe [25, 26]. Both mechanical (see, e.g., [2], Ch. 10) and laser processing [27] of ceramic materials proved to be extremely difficult. An additional fabrication challenge is attachment of the resonator to the ground plane or metallized dielectric substrate. Typically, epoxy is used but that approach adds a critical fabrication step, introduces uncertainty in impedance matching [2], and may bring an issue of reliability.

In this paper, we propose a DRA resonator that is formed by multiple individual building blocks. We refer to the proposed antenna type as a compound DRA (cDRA) [28]. Apart from design flexibility for the resonator shape, the cDRA's resonator can be built around the probe, avoiding the need for drilling. This alleviates some of the fabrication problems outlined above. If in addition glueless attachment [29] of the resonator building blocks to the grounded substrate is applied via pre-drilled holes, such an antenna can be made reconfigurable by manually removing or adding a certain number of building blocks. Furthermore, we show that the insertion depth of each resonator component can be used as yet another design parameter. Unlike [22], we use cylindrical building blocks in a 2D rather than volumetric grid which is more practical and easier to implement. Similarly, solid components of the resonator are easier to handle than, e.g., changing the liquid level in water-filled antennas [30].

A relevant concept has been explored recently [31, 32], where a perforated high permittivity substrate was used as a DRA's resonator, with cylindrical holes filled with either high ($\epsilon = 20$) or low (air) material to locally change the effective permittivity. In our approach, however, we use low cost pre-fabricated building blocks to form the resonator. In addition, the substrate can be any low loss material or even metal foil and no multi-layer structure for slot coupling is needed. Hence, the main goal of this study is to combine resonator's shape optimization with low fabrication complexity to achieve DRA's reconfigurability. Below, we present a few selected examples of a probe-fed cDRA. In Section 2, we discuss the design parameters and the corresponding numerical approach used to identify the appropriate resonator shapes and optimize the probe length. Experimental prototypes and measurement results are described in Section 3, while radiation patterns of several cDRAs are presented in Section 4. Section 5 concludes the paper.

* Corresponding author: Alexander P. Volkov (volkova@corning.com).

2. ANTENNA DESIGN

The concept of cDRA is shown in Fig. 1, where the DRA's resonator is formed by a group of cylindrical building blocks. For practical implementation, readily available yttrium stabilized zirconia cylinders with permittivity $\epsilon = 29$ and loss tangent $\tan\delta = 7 \times 10^{-3}$ [33] were selected. The cylinder's diameter and height above the ground plane were $d = 2.5$ mm and $h = 8.2$ mm, respectively. For a DRA to operate in a range of 7–12 GHz, the size of resonator with such permittivity should amount to ~ 10 mm [1, 2], so it would consist of < 10 cylinders. Hence, the antenna's resonator formed by up to 7 cylinders placed on a triangular grid of pre-drilled holes in the substrate was assumed. The cylinders were attached to a grounded (17 μm copper) FR-4 substrate (size 150 mm × 150 mm, thickness $t = 1.6$ mm, permittivity 4.3, loss tangent 0.022). The probe diameter is $d_p = 1.3$ mm, which is common for SMA connectors, with variable length L_p measured above the top (metal-free) substrate surface. The center-to-center distance for zirconia cylinders, $g = 3.06$ mm, was chosen to minimize the gap between the building blocks of the resonator. The distance between the probe center and the center of middle cylinder (position 4 in Fig. 1) was $p = 3.87$ mm.

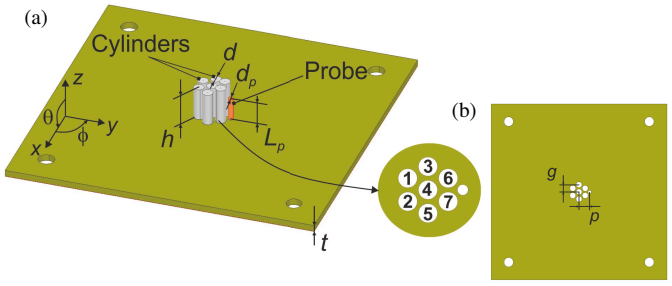

FIGURE 1. Example of probe-fed cDRA: (a) 3D view, (b) top view of the substrate with holes drilled to hold dielectric cylinders that form the resonator. The inset shows the numbering notation for the location of cylinders. Typical dimensions, discussed in Section 2 are as follows: $d = 2.5$ mm, $h = 8.2$ mm, $g = 3$ mm, $p = 3.9$ mm, $d_p = 1.3$ mm, $L_p = 5$–8 mm.

The following analysis was used to identify the probe length allowing the maximum number of potential cDRA operation states. Since any of 7 cylinders can either be present or absent, the maximum of $2^7 = 128$ combinations, including the case with no resonator present. To distinguish between different combination of building blocks that form the cDRA, the present and absent cylinders are marked by '1' or '0', respectively. The order of each position is shown in the inset of Fig. 1(a). For example, a cDRA with a cylinder missing at position 2 is labeled 1011111. This label can be interpreted as a map to envision the structure of each cDRA. The corresponding binary number can be converted for convenience to decimal format ($1011111 \rightarrow 95$) which we use as configuration index to refer to a particular map (cf. Fig. 3).

Analytical treatment of DRAs is only possible for a handful of basic shapes like hemispherical resonators [34, 35]. In our design optimization, we therefore rely on a finite element (Ansys HFSS) numerical model. In computations, the frequency grid was nonuniform to better resolve narrow resonances. The model was built to accurately represent the prototypes described in Section 3. For this, more subtle effects were considered. For example, the height of closest to probe cylinders (6 and 7, see inset in Fig. 1) was assumed 8.8 mm to account for connector's teflon isolator around the central wire. To identify promising resonator configurations and to optimize the probe length, resonant frequency and bandwidth were calculated for all 127 combinations of zirconia cylinders. Fig. 3 shows resonance frequency f_0 and bandwidth, calculated from DRA efficiency, defined as the ratio of the radiated power and the incident power of the antenna, at the -0.5 dB level ($> 90\%$). The smaller number of plotted points in Figs. 3(a), (c) indicates that the compound DRA with this resonator shape and probe length has fewer configurations with total efficiency exceeding 90%. The optimum probe length is approximately $L_p = 5.5$ mm, as this length provides a larger number of possible resonator shapes for manual cDRA reconfigurability.

Several DRA configurations with different numbers of cylindrical building blocks (and having different resonant frequencies) have been selected based on the analysis presented in Fig. 3. These designs are shown in Fig. 2 with the corresponding configuration map. For convenience, we refer to them by the number of individual building blocks present in the resonator, DRAn, where $n = 7$, 5, 4, and 3. DRA7 has the largest resonator, with all 7 cylinders present. In DRA5, the center and one outer cylinder are removed. DRA4 has four cylinders and DRA3 — three, whereas in that latter case the distance from probe to the nearest cylinder is the largest. Fig. 4 shows total efficiencies versus frequency for all four configurations and different probe lengths. Again, one can conclude that $L_p = 5.5$ mm provides optimum performance. In that case, the operation bandwidth for DRA7, DRA5, DRA4 and DRA3 is 11%, 15%, 12%, and 11%, respectively.

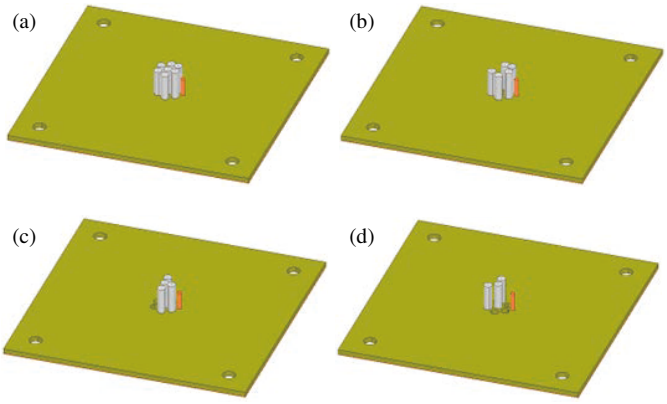

FIGURE 2. Four configurations of the probe-fed reconfigurable cDRA: (a) 1111111 or DRA7, (b) 0110111 or DRA5, (c) 0011101 or DRA4, and (d) 0111000 or DRA3.

3. PROTOTYPES AND MEASUREMENTS

A cDRA prototype for the four configurations of Fig. 2 was fabricated (Fig. 5) and characterized. The return loss was measured using an Agilent PNA Network Analyzer, model E8361A. The frequency ranged from 6 to 13 GHz with 201 sampling points at 1 kHz bandwidth. For additional model validation, mea-

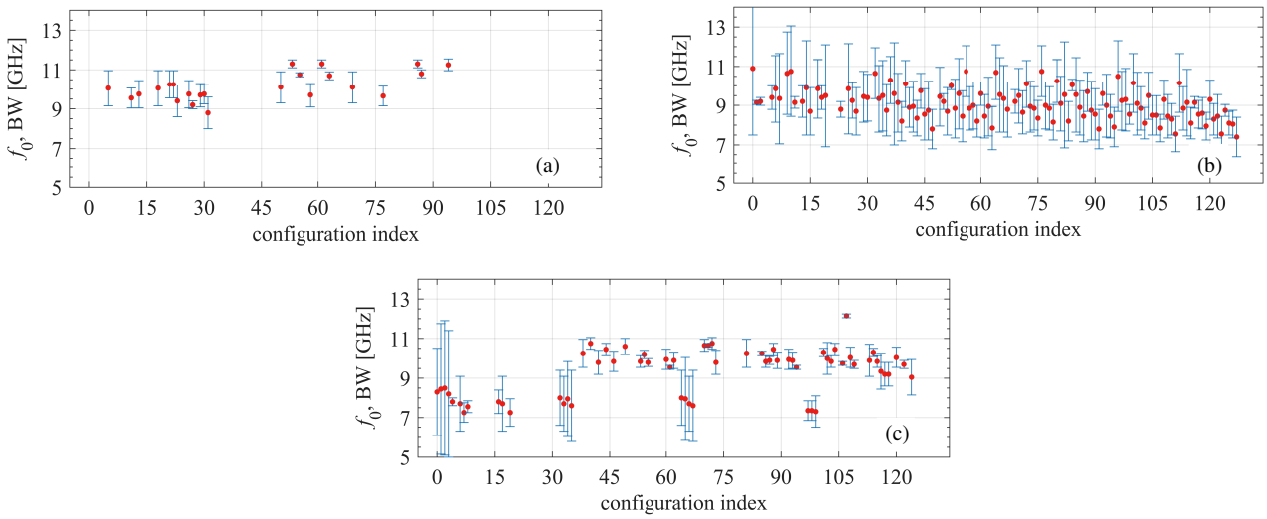

FIGURE 3. Resonant frequency (red dots) and bandwidth (blue bars) of various cDRAs vs. configuration index defined in the text. Results are only shown for configurations with total efficiency above 90%; (a) probe length $L_p = 3.5$ mm, (b) $L_p = 5.5$ mm, and (c) $L_p = 7.5$ mm.

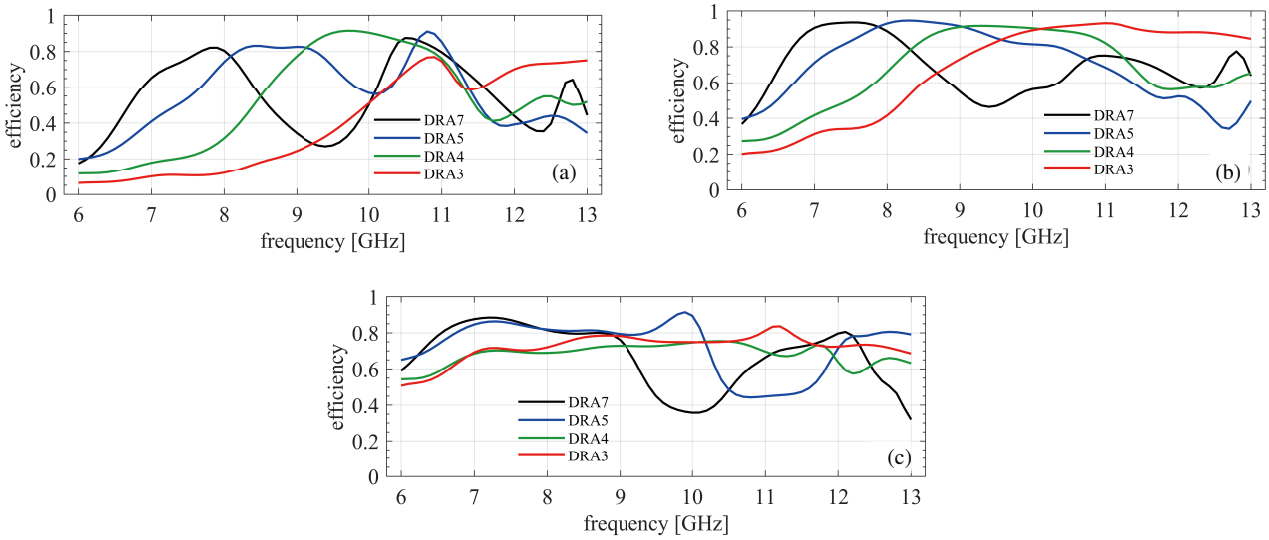

FIGURE 4. Calculated total efficiencies for resonator shapes of Fig. 2 with different probe lengths; (a) $L_p = 3.5$ mm, (a) $L_p = 5.5$ mm, (a) $L_p = 7.5$ mm.

surements have also been done for longer probes (8.5 mm and 7.5 mm) before the probe was finally cut to the optimal length of 5.5 mm. Measured and calculated values of the reflection coefficient $|S_{11}|$ are shown in Figs. 6(a)–(c). Good agreement between simulated and measured resonance frequencies and bandwidths can be observed. Longer than optimal probes tend to shift resonant peaks to higher frequencies and the overall performance of the DRA decreases. This trend has also been observed in a variety of solid-resonator DRAs [25, 26]. This effect is particularly pronounced for the small overall size of the resonator (DRA3, red curves in Fig. 6).

We note that agreement between measurements and simulations decreases with frequency, mostly because of increased sensitivity to fabrication imperfections. For this reason, higher-order, narrower resonances located at higher frequencies are especially difficult to accurately capture in the numerical model. It is also possible to identify operation conditions when multiple, closely located resonances merge to ensure broadband operation. One such example is DRA3 with $L_p = 5.5$ mm, which exhibits a bandwidth (at the -10 dB level) of about 3 GHz. The two close resonances are seen more clearly at the corresponding numerical curve (green dots in Fig. 6(a)). As a side remark, the fundamental resonant frequency can be estimated with reasonable accuracy of $\sim 5\%$ from the approximate characteristic size of the DRA resonator $a \sim \lambda_0/\sqrt{\epsilon} = c/(f_0\sqrt{\epsilon})$ [1], where $a \sim \sqrt[3]{V}$, with V being the volume of the compound resonator consisting of N cylinders, $V = N\pi d^2 h/4$; f_0 and λ_0 are the zero-order resonant frequency of a DRA and the corresponding wavelength, and c is the speed of light.

Figure 6(a) shows how changing the compound resonator configuration allows for tuning the lowest-mode resonant frequency f_0 from 7.5 GHz (DRA7) to 8.5 GHz (DRA5) to 9.5–10.5 GHz (two resonances merged for DRA4) or 11 GHz (DRA3). This mechanical reconfigurability can be achieved

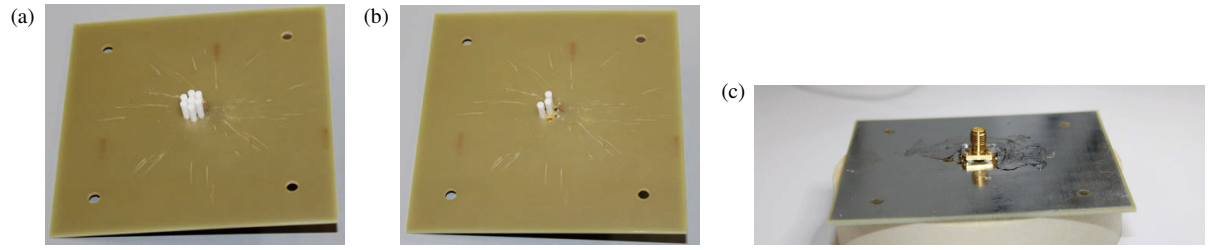

FIGURE 5. Experimental prototypes of a cDRA; (a) top view of cDRA7, (b) top view of cDRA3, (c) bottom view. The antenna is excited by coaxial probe which is an inner conductor of a SMA connector. Outer holes are intended for mounting of the cDRA assembly.

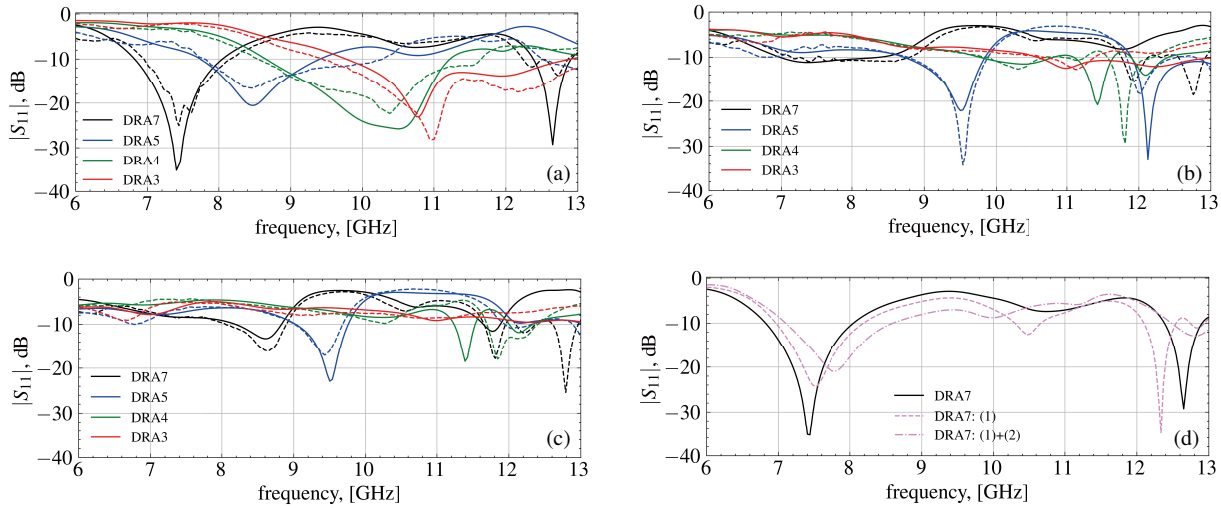

FIGURE 6. Calculated (solid curves) and measured (dashed curves) reflection coefficient $|S_{11}|$ for four cDRAs of Fig. 2; (a) $L_p = 5.5$ mm; (b) $L_p = 7.5$ mm; (c) $L_p = 8.5$ mm; (d) DRA7 with $L_p = 5.5$ mm when cylinder (dashed curve) or cylinder and (dash-dotted) pushed through the substrate by 4 mm.

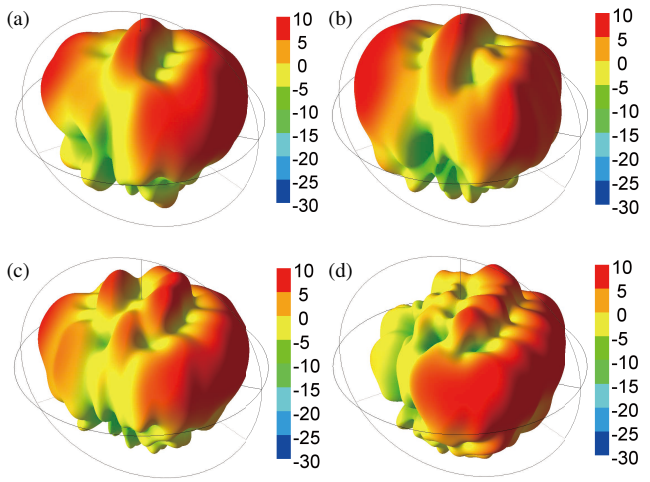

FIGURE 7. cDRA radiation pattern (dBi) for different resonator shapes: (a) DRA7 at 7.5 GHz, (b) DRA5 at 8.5 GHz, (c) DRA4 at 10 GHz, and (d) DRA3 at 11.5 GHz; $L_p = 5.5$ mm.

by simply removing several cylinders from DRA7. Fine tuning of resonant frequency can be achieved by pushing ceramic cylinders deeper through the substrate during the installation stage. In this way one can reduce the effective size (amount of dielectric material above the ground plane) of the resonator.

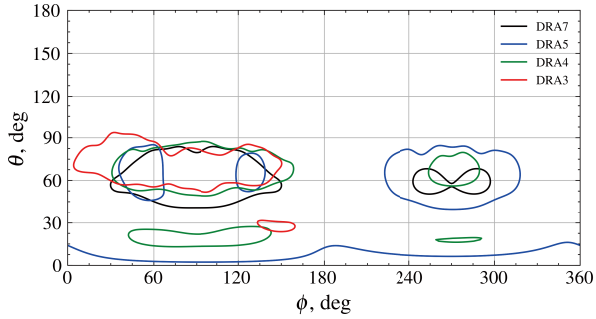

FIGURE 8. 3-dB beam contours: DRA7 at 7.5 GHz, DRA5 at 8.5 GHz, DRA4 at 10.0 GHz, DRA3 at 11.5 GHz.

An example of resonant frequency tuning is shown in Fig. 6(d), where cylinders 1 or/and 2 of DRA7 are pushed 4 mm deeper through the substrate. This resulted in forward (backward) resonance frequency shift of the first (second) resonant mode.

Changing the shape of the cDRA by adding or removing the resonator's building blocks affects the resonant frequency and to lesser extent the antenna's bandwidth and gain. Table 1 shows the characteristics of the considered cDRA configurations. However, the DRA's radiation pattern also strongly depends on the resonator shape.

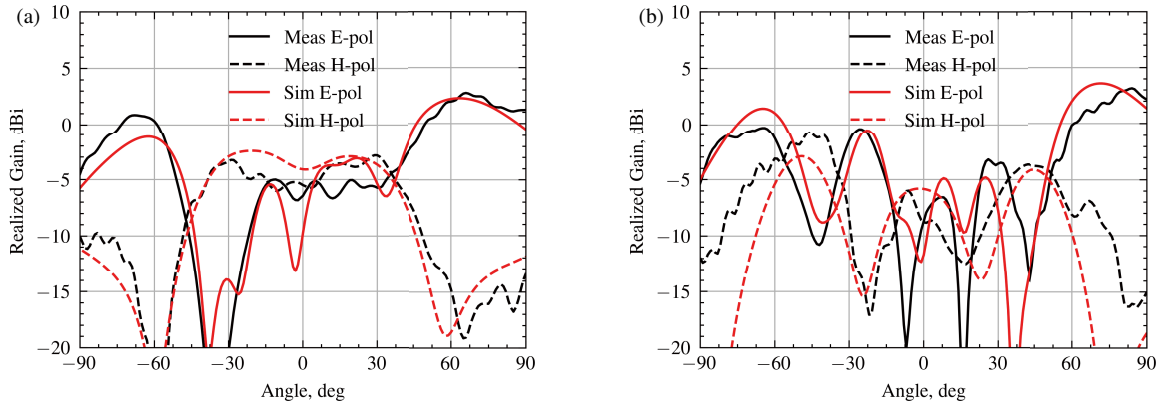

FIGURE 9. Calculated vs. measured radiation pattern for DRA3: (a) 9.5 GHz, (b) 11 GHz; $L_p = 5.5$ mm.

TABLE 1. cDRA characteristic.

cDRA	f_c, GHz	G_0, dBi	min($\|S_{11}\|$), dB	BW, GHz
DRA7	7.5	7.36	−35.2	6.85...8.05
DRA5	8.55	6.35	−20.5	7.75...9.43
DRA4	9.93	6.4	−25.7	8.66...11.21
DRA3	11.32	7.01	−23.05	9.78...12.87

4. RADIATION PATTERNS

Figure 7 shows calculated radiation patterns for cDRAs of Fig. 2 plotted in the spherical coordinate system of Fig. 1. The cDRAs exhibit monopole-like radiation patterns due to the probe-fed seeding structure. DRA7 (Fig. 7(a)) exhibits a symmetric (with respect to the Y-Z plane) radiation pattern which is expected due to the compound resonator's Y-Z plane symmetry. The main beam is relatively wide in the azimuthal direction (120°) and is directed along the positive Y-axis. The maximum directivity is 7.7 dBi in the two directions (ϕ, θ), namely (70°, 60°) and (110°, 60°). Switching between DRA7 to DRA5 not only changes resonant frequency, but also direction of the main beam. For DRA5 (Fig. 7(b)) two asymmetric narrower lobes are pointing in the (50°, 60°) and (130°, 60°) directions and have a width of 30°. The maximum directivity is 6.5 dBi. The radiation pattern of DRA4 (Fig. 7(c)) is quasi-symmetric due to the symmetry of the three closest cylinders to the probe. It resembles the radiation pattern of DRA7: two close beams (90° ± 10°, 70°) form a ∼ 120° beam with maximum directivity of 6.8 dBi. Finally, DRA3 has an asymmetric radiation pattern with beamwidth of (140°) and directivity of 7.4 dBi. We therefore conclude that some configurations largely maintain their radiation pattern, only changing resonance frequency, e.g., DRA7↔DRA4, while others may change the direction and width of the main beam. Fig. 8 illustrates the aforementioned using 3-dB beam contours plotted in polar coordinates for the considered cDRA configurations. Fig. 9 shows measured and calculated patterns for DRA3 plotted as a function of polar angle. We obtained reasonable agreement between calculated and measured values for both off-resonance and resonant frequencies.

5. CONCLUSIONS

We proposed a reconfigurable, compound-resonator DRA based on readily available dielectric shapes, like glass or ceramic beads or cylinders, as building blocks of the cDRA. Such blocks can be placed around the preinstalled probe, thus eliminating the need for drilling glass or ceramics. We demonstrated feasibility of the proposed approach using zirconia cylinders to form the antenna resonator. Depending on the number and position of these cylinders, various resonant wavelengths and radiation patterns of the antenna can be achieved. Unlike the conventional approach of gluing the resonator to the substrate, our prototypes relied on snapfit of the building block cylinders to a grounded dielectric substrate via pre-drilled holes. Good agreement between predicted and measured resonant frequencies and bandwidths of the four considered antennas was observed. The approach offers flexibility of the DRA's design through resonator shape. Antenna's reconfigurability can be achieved via changing the number and position of the cDRA's building blocks, as well as varying the insertion depth of each building block. The approach can be extended to a larger number of building blocks and more complex resonator shapes. Although the considered cDRA was excited by a coaxial probe placed outside the block of cylinders, similar designs were tested when the probe was placed inside the compound resonator.

REFERENCES

[1] Luk, K. M. and K. W. Leung, *Dielectric Resonator Antennas*, Research Studies Press, 2003.

[2] Petosa, A., *Dielectric Resonator Antenna Handbook*, Artech House, 2007.

[3] Chen, Z., J.-Y. Deng, and H. Liu, *Dielectric Resonator Antennas: Materials, Designs and Applications*, John Wiley & Sons, 2023.

[4] Soren, D., R. Ghatak, R. K. Mishra, and D. Poddar, "Dielectric resonator antennas: Designs and advances," *Progress In Electromagnetics Research B*, Vol. 60, 195–213, 2014.

[5] Basile, V., M. Grande, V. Marrocco, D. Laneve, S. Petrignani, F. Prudenzano, and I. Fassi, "Design and manufacturing of super-shaped dielectric resonator antennas for 5G applications using stereolithography," *IEEE Access*, Vol. 8, 82 929–82 937, 2020.

[6] Zhang, Y., S. Ogurtsov, V. Vasilev, A. A. Kishk, and D. Caratelli, "Advanced dielectric resonator antenna technology for 5G and 6G applications," *Sensors*, Vol. 24, No. 5, 1413, 2024.

[7] Parvathi, V. L., A. Rajput, R. B. Raut, and B. Mukherjee, "A novel low-profile rectangular dielectric resonator antenna with enhanced gain for 5G new radio band applications," *Microwave and Optical Technology Letters*, Vol. 65, No. 9, 2572–2580, 2023.

[8] Khan, M. U., A. Muhammad, M. S. Sharawi, M. Alathbah, *et al.*, "Singly-fed large frequency ratio composite dielectric resonator antenna for sub-6 GHz and mm-Wave 5G applications," *IEEE Access*, Vol. 12, 67 837–67 846, 2024.

[9] Yan, N., H. Yuan, Y. Luo, and K. Ma, "A wideband millimeter-wave circularly polarized dielectric resonator antenna with a stacked strip using SISL technology for 5G applications," *IEEE Antennas and Wireless Propagation Letters*, Vol. 24, No. 1, 262–266, 2025.

[10] Halimi, M. A., T. Khan, D. Surender, N. Nasimuddin, and S. R. Rengarajan, "Dielectric resonator antennas for RF energy-harvesting/wireless power transmission applications: A state-of-the-art review," *IEEE Antennas and Propagation Magazine*, Vol. 66, No. 1, 34–45, 2024.

[11] Li, C.-H. and T.-Y. Chiu, "340-GHz low-cost and high-gain on-chip higher order mode dielectric resonator antenna for THz applications," *IEEE Transactions on Terahertz Science and Technology*, Vol. 7, No. 3, 284–294, 2017.

[12] Singhwal, S. S., L. Matekovits, I. Peter, and B. K. Kanaujia, "A study on application of dielectric resonator antenna in implantable medical devices," *IEEE Access*, Vol. 10, 11 846–11 857, 2022.

[13] Kishk, A. A., X. Zhang, A. W. Glisson, and D. Kajfez, "Numerical analysis of stacked dielectric resonator antennas excited by a coaxial probe for wideband applications," *IEEE Transactions on Antennas and Propagation*, Vol. 51, No. 8, 1996–2006, 2003.

[14] Misala, S. and S. A. Mosa, "A novel stacked rectangular with surface mounted short rectangle dielectric resonator antenna in C-band applications," *Progress In Electromagnetics Research Letters*, Vol. 115, 81–89, 2023.

[15] Chair, R., S. L. S. Yang, A. A. Kishk, K. F. Lee, and K. M. Luk, "Aperture fed wideband circularly polarized rectangular stair shaped dielectric resonator antenna," *IEEE Transactions on Antennas and Propagation*, Vol. 54, No. 4, 1350–1352, 2006.

[16] Liang, X.-L. and T. A. Denidni, "H-shaped dielectric resonator antenna for wideband applications," *IEEE Antennas and Wireless Propagation Letters*, Vol. 7, 163–166, 2008.

[17] Chen, Z., Y.-T. Liang, K. X. Wang, and T. Yuan, "A dielectric resonator antenna with enhanced gain bandwidth," *IEEE Transactions on Antennas and Propagation*, Vol. 72, No. 10, 8034–8039, 2024.

[18] Whiting, E. B., S. D. Campbell, G. Mackertich-Sengerdy, and D. H. Werner, "Dielectric resonator antenna geometry-dependent performance tradeoffs," *IEEE Open Journal of Antennas and Propagation*, Vol. 2, 14–21, 2020.

[19] Dhar, S., R. Ghatak, B. Gupta, and D. R. Poddar, "A wideband Minkowski fractal dielectric resonator antenna," *IEEE Transactions on Antennas and Propagation*, Vol. 61, No. 6, 2895–2903, 2013.

[20] Gangwar, K., A. Sharma, G. Das, and R. K. Gangwar, "Investigation on novel wideband fractal antenna design based on cylindrical shape dielectric resonator," *International Journal of RF and Microwave Computer-Aided Engineering*, Vol. 29, No. 11, e21943, 2019.

[21] Gaonkar, A., M. Ayyappan, and P. Patel, "A novel fractal RDRA for C-band applications," *IEEE Transactions on Components, Packaging and Manufacturing Technology*, Vol. 13, No. 7, 995–1002, 2023.

[22] Alroughani, H. and D. A. McNamara, "The shape synthesis of dielectric resonator antennas," *IEEE Transactions on Antennas and Propagation*, Vol. 68, No. 8, 5766–5777, 2020.

[23] Chen, Z. N., *Handbook of Antenna Technologies*, 661–697, Springer Singapore, 2014.

[24] Oh, Y., V. Bharambe, B. Mummareddy, J. Martin, J. McKnight, M. A. Abraham, J. M. Walker, K. Rogers, B. Conner, P. Cortes, E. MacDonald, and J. J. Adams, "Microwave dielectric properties of zirconia fabricated using nanoparticle jetting™," *Additive Manufacturing*, Vol. 27, 586–594, 2019.

[25] Leung, K. W., K. M. Luk, K. Y. A. Lai, and D. Lin, "Theory and experiment of a coaxial probe fed hemispherical dielectric resonator antenna," *IEEE Transactions on Antennas and Propagation*, Vol. 41, No. 10, 1390–1398, 1993.

[26] Junker, G. P., A. A. Kishk, and A. W. Glisson, "Input impedance of dielectric resonator antennas excited by a coaxial probe," *IEEE Transactions on Antennas and Propagation*, Vol. 42, No. 7, 960–966, 1994.

[27] Gopal, P. M., V. Kavimani, K. Gupta, and D. Marinkovic, "Laser-based manufacturing of ceramics: A review," *Micromachines*, Vol. 14, No. 8, 1564, 2023.

[28] Kobyakov, A., A. Volkov, D. R. Peters, and T. Ren, "Mechanically reconfigurable dielectric resonator antenna," in *2024 IEEE International Symposium on Antennas and Propagation and INC/USNC-URSI Radio Science Meeting (AP-S/INC-USNC-URSI)*, Firenze, Italy, Jul. 2024.

[29] Sarkar, C., D. Guha, and C. Kumar, "Glueless compound ground technique for dielectric resonator antenna and arrays," *IEEE Antennas and Wireless Propagation Letters*, Vol. 16, 2440–2443, 2017.

[30] Zhu, J., L. Xing, Q. Xu, and D. Yan, "Sensitivity measurement of a pattern reconfigurable water antenna in IoT applications," in *2020 International Conference on Microwave and Millimeter Wave Technology (ICMMT)*, 1–3, Shanghai, China, Sep. 2020.

[31] Kremer, H. I., K. W. Leung, and M. W. K. Lee, "Compact wideband low-profile single- and dual-polarized dielectric resonator antennas using dielectric and air vias," *IEEE Transactions on Antennas and Propagation*, Vol. 69, No. 12, 8182–8193, 2021.

[32] Tong, C., H. I. Kremer, N. Yang, and K. W. Leung, "Compact wideband circularly polarized dielectric resonator antenna with dielectric vias," *IEEE Antennas and Wireless Propagation Letters*, Vol. 21, No. 6, 1100–1104, 2022.

[33] Lanagan, M. T., J. K. Yamamoto, A. Bhalla, and S. G. Sankar, "The dielectric properties of yttria-stabilized zirconia," *Materials Letters*, Vol. 7, No. 12, 437–440, 1989.

[34] Leung, K. W., "General solution of a monopole loaded by a dielectric hemisphere for efficient computation," *IEEE Transactions on Antennas and Propagation*, Vol. 48, No. 8, 1267–1268, 2000.

[35] Kobyakov, A., "Fully analytical formula for input impedance of center-fed hemispherical dielectric resonator antenna," in *2023 IEEE International Symposium on Antennas and Propagation and USNC-URSI Radio Science Meeting (USNC-URSI)*, 1169–1170, Portland, OR, USA, Jul. 2023.